

# Integrated Actuation and Self-Sensing for Twisted-and-Coiled Actuators with Applications to Innervated Soft Robots

Jiefeng Sun<sup>1</sup> and Jianguo Zhao<sup>1</sup>

**Abstract**—Traditional soft robots require separate sensors and actuators to precisely control their motion. A twisted-and-coiled actuator (TCA) is a new artificial muscle with both actuation and self-sensing capability that can simultaneously serve both as a sensor and an actuator allowing to control the motion of TCAs without external sensors. This paper investigates the integrated sensing and actuation for TCAs, and the self-sensing function is realized by only measuring the TCA’s electrical resistance change. The closed-loop control of a single TCA is realized, and an innervated soft finger that can respond to external load without extra sensors is demonstrated. Our results will lay a foundation for integrated sensing and control by directly using the actuator, paving the way for self-contained smart robotic systems (e.g., untethered soft robots).

## I. INTRODUCTION

Soft robots’ actuation and sensing are often separated: soft actuators are used to generate motion, and extra soft sensors to feedback their state information, e.g., velocity, displacement, and temperature. Integrating sensing and actuation on the same actuator – using the same actuator both as an actuator and a sensor at the same time, is intriguing, especially for soft robots that have small sizes [1].

A twisted-and-coiled actuator (TCA) is a promising artificial muscle that exhibits both actuation and self-sensing capabilities, which has been investigated separately. For actuation, they have been used to actuate robotic hands/grippers [2], morphing mechanisms [3] and prosthetic devices [4]. For self-sensing, the change of the electrical resistance is studied when a TCA is used as a sensor [5], [6] and as an actuator [7].

With the actuation and self-sensing capability, it is intriguing to see if we can combine them together to enable closed-loop control. Such a topic is under-explored, with only Ref. [8], [9] realizing the closed-loop control of a TCA during actuation. However, the method is only verified on TCAs made of fishing lines (may not work on TCAs made of other materials), and the closed-loop control of the TCA is not used for actuating a robot.

In this paper, we aim to accomplish an integrated actuation and sensing scheme for TCAs made from conductive sewing threads [10] as illustrated in Fig. 1(a), with the ultimate goal of realizing self-contained untethered soft robotic systems that will not rely on bulky external sensors [11], [12] for

\*This work is partially supported by the National Science Foundation under Grant CNS-1755766.

<sup>1</sup>Jiefeng Sun, and Jianguo Zhao are with the Department of Mechanical Engineering at Colorado State University, Fort Collins, CO, 80523, USA. J.Sun@colostate.edu, jianguo.zhao@colostate.edu

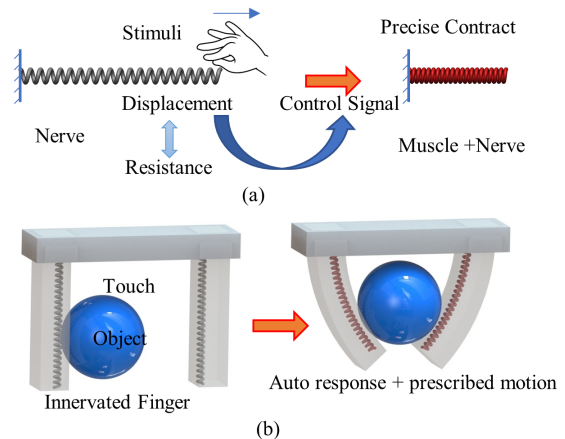


Fig. 1: (a) The artificial muscle TCA can accordingly response to external stimuli. (2) The innervated soft finger actuated by the TCA.

the closed-loop control. In this work, there are two key points for the scheme: 1) when not actuated, the TCA can sense environmental stimuli and works as a sensor (nerve). 2) When actuated, the TCA works as a sensor and actuator (nerve and muscle). By integrating the two functions, we achieved innervated robots as illustrated in Fig. 1(b). The basic principle is to infer the state (displacement or force) from the resistance of the TCA and then use it as a feedback signal to control the state. Compared with [8], [9], our method does not involve modeling and parameter identification for the model; instead, it only needs to characterize a resistance-displacement relationship, which can be used for a TCA of any length with the same fabrication parameters.

However, it is difficult to use the resistance of TCAs fabricated by existing approaches for sensing purposes. Some fabrication methods will result in random resistance when a TCA is actuated because the coils in it will randomly contact each other. For example, the bundled TCAs have coils touching each other all the time [12], [13], and TCAs fabricated using conventional methods (self-coiling or mandrel coiling) will have coils contacting each other soon after it is actuated due to the limited stroke.

To address the problem, we recently developed a new method to fabricate TCAs that can generate sufficient stroke before coil contact [14]. For these TCAs, their displacements can be inferred from the resistance change during actuation, and thus the closed-loop control of the displacement could be realized by using the resistance as feedback. Further, after

embedding the TCA into a soft body, we demonstrate the closed-loop shape control of a soft robotic finger.

Our work has two main contributions. First, we discover that the resistance change of the upgraded TCA is continuous and monotonic which can be used to infer its displacement or force. Second, to our best knowledge, we are the first to implement a closed-loop control only using resistance as feedback for TCAs made of conductive sewing threads. TCAs are embedded in soft materials to demonstrate an innervated soft finger that can be triggered by external loads and controlled to bend precisely.

The rest of the paper is organized as follows. We first introduce the fabrication of the upgraded TCA in Section II. Then, we characterize TCAs with and without actuation in Section III. After that, we conduct the closed-loop control of a single TCA in Section IV. Finally, in Section V, the innervated soft finger is demonstrated.

## II. NEW FABRICATION METHOD

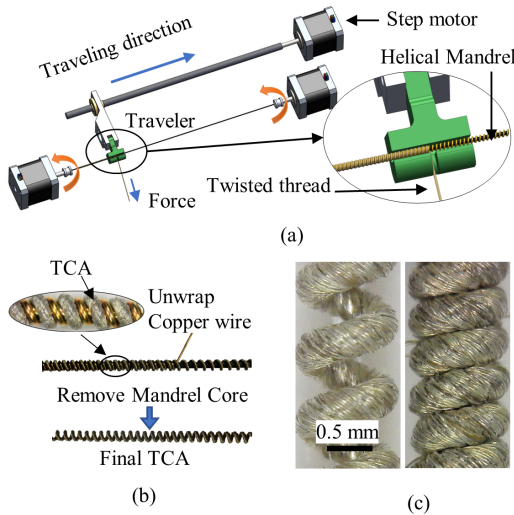


Fig. 2: Fabrication process of the TCA. (a) Coiled the twisted fiber on the helical mandrel. (b) Remove the TCA from the mandrel after annealing. (c) Microscopic photos of the TCA in room temperature (left) and after being heated up (right).

The main difference between conventional TCAs and our TCAs with resistance self-sensing is that the upgraded TCA has a larger stroke that prevents early coil contact [14]. The basic principle is to use a helical mandrel that fixes the TCA into a helical shape with large gaps between coils and anneal it in that shape to impose the gaps between coils. The precursor twisted fiber for the TCA should be a single ply of the conductive sewing thread. Otherwise, the resistance of the TCA will be random due to the irregular direction of silver-painted yarns.

There are 6 steps to fabricate our TCA [14]. 1) Fabricate a twisted fiber with 1-ply thread. 2) Fabricate a helical mandrel. 3) Coil the twisted fiber on the helical mandrel as in Fig. 2(a). 4) Anneal the whole assembly in an oven ( $185^{\circ}\text{C}$ ). 5) Remove the TCA from the mandrel as shown

in Fig. 2(b). 6) A training process (several heating cycles) is performed to endow the TCA with consistent performance.

Gaps are imposed on the fabricated TCA between the neighboring coils that allow the TCA to have a larger stroke 35.7% even there is no weight hanged (preloading). The microscopic photos of the un-actuated and actuated TCA are shown in Fig. 2(c). After the training process, the TCA's length will have a natural length  $l_n$ , which will be shorter than the length when the mandrel is not removed. The main parameters for the fabricated TCAs are as follows: twisted fiber length 350 mm, twisted fiber diameter 0.34 mm, TCA outer diameter 1.08 mm, TCA natural length 110 mm, made length 133.5 mm, unit resistance  $6.7 \Omega/\text{dm}$

## III. CHARACTERIZATION OF THE SELF-SENSING CAPABILITY

To understand how the resistance can reflect the displacement of a TCA, we first discuss the parameters that influence the resistance.

### A. Dependence of the Resistance on Other Parameters

The conductive sewing thread is conductive due to the silver traces painted on the yarns. According to existing modeling work of TCAs [12], [15], the thermal-mechanical relationship can be expressed as a nonlinear function

$$f(\Delta T, \Delta x, F, \dot{x}) = 0 \quad (1)$$

where  $\Delta T$  is the temperature change,  $\Delta x$  the displacement,  $F$  the external load, and  $\dot{x}$  the velocity of the actuation. For example, a first-order function is  $k\Delta x + b\dot{x} + c\Delta T - F = 0$ , where  $k$ ,  $b$  and  $c$  are respectively the TCA's stiffness, damping coefficient, and temperature contribution coefficient ( $\text{N}/^{\circ}\text{C}$ ) [12].

The TCA's resistance  $R$  can be expressed as a nonlinear function in terms of the variables  $\Delta T$ ,  $\Delta x$  and  $F$  [7].

$$R = g(\Delta T(\Delta x, F), \Delta x, F) = h(\Delta x, F) \quad (2)$$

In Eq. (2), the viscous effect is ignored due to its small quantity. We express the temperature as a function related to  $\Delta x$  and  $F$ , and thus  $\Delta T$  is treated as an intermediate variable so that  $R$  can be fully determined by  $\Delta x$  and  $F$ . When a TCA only works as a sensor, Eq. (2) can be further simplified because  $\Delta x$  will then merely depend on  $F$ . When the TCA is heated up, given a constant external force  $F$ , the relationship between the other two variables ( $R$  and  $\Delta x$ ) can be obtained from experiments. Similarly, given a fixed  $\Delta x$ , the relationship between the ( $R$  and  $F$ ) can be obtained.

### B. Resistance-Length (R-L) and Resistance-Displacement (R-D) Relationship of an Actuated TCA with a Given Load

The most common scenario for a given  $F$  is to lift a weight using a TCA. For such a case,  $F$  is approximately equal to the gravity of the weight because the maximum acceleration of the weight is  $0.2 \text{ m/s}^2$  in our experiments, which is negligible ( $< 3\%$ ) compared to the gravity.

A driving-sensing module (DSM) is shown in Fig. 3 that can: 1) characterize the TCA; 2) conduct the feedback

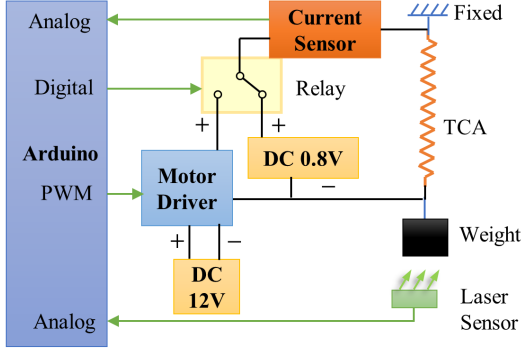


Fig. 3: The setup used to measure the resistance-length relationship and control the TCA and the robotic finger

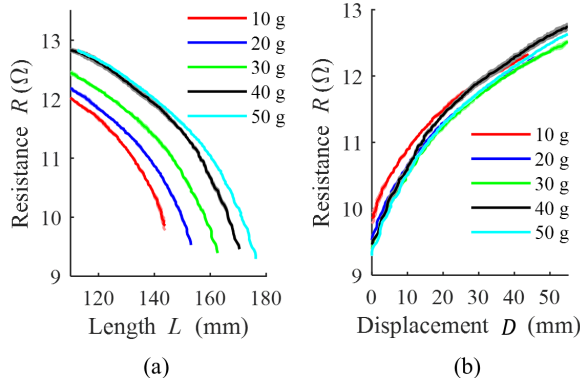


Fig. 4: (a) The resistance-length relationship for different weights. (b) The resistance-displacement relationship for different weights.

control experiments. The DSM can switch between two separate circuit loops using a relay module. The first loop that can conduct the feedback control comprises a motor driver (Pololu MC33923) and a high side voltage-current sensor (Adafruit INA 219, accuracy 1%, resolution 0.8 mA), and the second loop with a smaller DC power source is only for sensing when TCA is not actuated.

In the experiments, a TCA ( $l_n = 110$  mm) is hanged with a weight at its bottom end and a laser displacement sensor (OPT2006, Wenglor sensoric GmbH) faces the bottom of the weight to measure its displacement. The motor driver, the current sensor, and the laser sensor connect to an Arduino Uno board to synchronize all the signals. There are two variables in the experiments: the weights and the actuation velocity. For each weight (10, 20, 30, 40, and 50 g), we actuate the TCA with different velocity using constant voltages (12 or 10 V).

Figure 4 shows the R-L and R-D relationship (the average of three repeated experiments) using  $U = 12$  v. It is obvious that the resistance gradually increases when the TCA contracts, and the R-L relationship is continuous and monotonic, indicating the resistance can uniquely reflect a TCA's length. It is observed that the R-L relationships for  $U = 10$  V (not shown in Fig. 4) are almost the same with  $U = 12$  V for the same weight, which implies that actuation

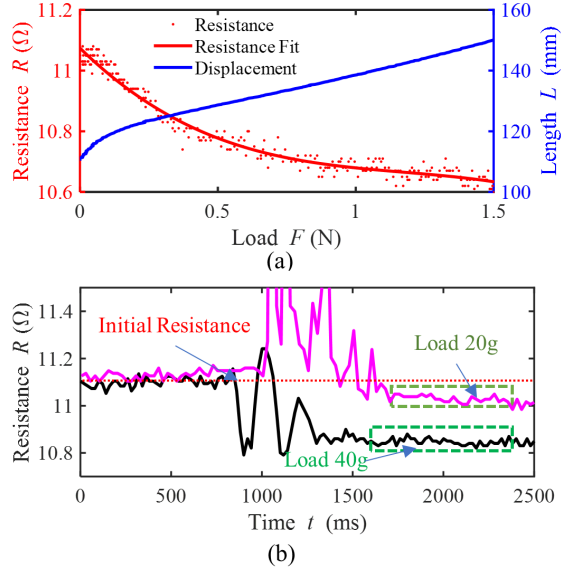


Fig. 5: (a) The resistance and the length with respect to the applied force when the TCA is not actuated. (b) The response of the resistance when 20 g or 40 g is applied on the end of the TCA.

velocity has negligible influence on the R-D relationship, therefore the relationship is applicable for holding function (velocity reaches 0), which will be discussed in Section IV. Furthermore, the R-D curves corresponding to different weights almost overlap with each other as shown in Fig. 4 (b), which implies that the R-D relationship is not sensitive to the weight when the stress is less than 70% of the breaking stress of the TCA (7.7 MPa). So, the same R-D curve can be used to approximately control the displacement of the TCA even when the weight is unknown.

### C. Un-actuated TCA as a Load Sensor

When the TCA is not actuated, it can be used as a load sensor [5], [6]. To characterize its capability, the TCA's resistance and the reaction force are measured by pulling the TCA longer using a force stand (ESM 303 with M5-12 force gauge, Mark-10 Inc.) with a constant speed (5 mm/s). The displacement and force are sampled and the TCA's resistance is also measured by applying a 0.8 V voltage on it. The voltage will only increase the TCA's temperature 1-2 °C (Obtained by FLIR E8 Infrared Camera).

Figure 5(a) shows that the resistance and the length of the TCA change with respect to the applied force. It shows the resistance decreases when the force increases. Based on the principle, the load applied can be determined by the amount of the resistance change. Figure 5(b) shows the resistance change with respect to the time when a 40 g and a 20 g are instantly applied at the end of the TCA. To distinguish different loads, the vibration is ignored and the load will be confirmed when a lower resistance is continuously sensed as shown in the green boxes of Fig. 5(b). After sensing the different loads, the TCA can respond according to the load, for example, lift

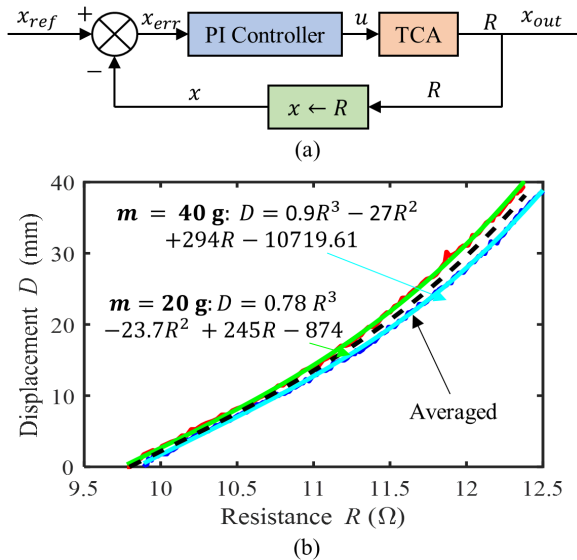


Fig. 6: (a) Schematic of the PI control. (b) The fitted D-R curve for 20 g and 40 g used in the the feedback control.

40 mm when a 40 g is applied (section IV and the supporting video: <https://youtu.be/WyPtp2IQqPo>).

#### IV. CLOSED-LOOP CONTROL USING SELF-SENSING

With the R-D relationship, the displacement-resistance (D-R) relationship is obtained to enable the closed-loop control of the displacement using a PI controller. Combining the sensing capability when the TCA is and is not actuated, the innervated TCA can sense external stimuli and respond to it.

##### A. Closed-loop Control of the TCA's Displacement

As shown in Fig. 6(a), the control loop is closed on the error between a reference displacement and the displacement calculated from the measured resistance using the D-R relationship. The D-R curves for 20 g and 40 g are fitted with a third-order polynomial. As shown in Fig. 6(b), the root-mean-square error (RMSE) for the two curves are respectively: 0.2184 mm and 0.3486 mm. When the averaged curve of the two curves (20 g and 40 g) is used, there will be a maximum steady-state difference less than  $\pm 20\%$  for step-response experiments compared with the case using the specific curve. It is not difficult to know the weight because the sensing function described in Section III-C allows us to know the approximate weight (20 or 40 g) if the resistance is monitored when adding the weight. But to realize a precise control, the following studies use the specific D-R curve corresponding to the weight.

A digital filter (Modified moving average method) is used to obtain the equivalent moving average of the current to calculate the resistance. Also, the current sensor has an internal ADC based on a delta-sigma ( $\Delta\Sigma$ ) front-end with a 500kHz typical sampling rate that has good noise rejection.

We find that an integral controller is necessary to reduce the steady-state error since the TCA has to be actuated to maintain the target position. Figure 7(a) shows the step

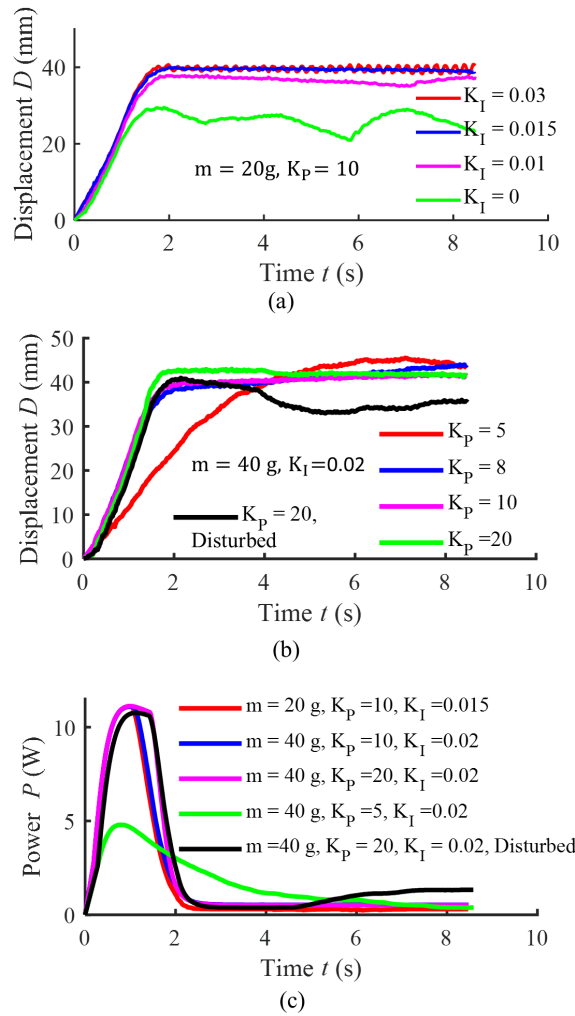


Fig. 7: (a) Step response of the displacement with a wight of 20 g using  $K_p = 10$  and different  $K_I$ . (b) Step response of the displacement with a wight of 40 g using  $K_I = 0.02$  and different  $K_p$ . (c) The input power for the step response experiments.

response (40 mm) of the TCA lifting 20 g when  $K_p = 10$  is used for all cases. When  $K_I = 0$ , the steady-state error  $e_s \approx 30\%$  and when  $K_I = 0.01$ , the  $e_s$  is reduced to around 12%. We find the optimal  $K_I$  to be 0.015 that can maintain the  $e_s < 5\%$ . However, when  $K_I$  is too large (e.g., 0.03), the system starts to oscillate (see the supporting video).

The influence of the  $K_p$  is studied using a step response (40 mm) of the TCA lifting 40 g in Fig. 7(b). A larger  $K_I = 0.02$  is used to suppress the steady-state error to be less than 5%. When  $K_p = 5$ , the rising time is longer and there is a little overshoot because the  $K_I = 0.02$  is relatively large for this  $K_p$ . When  $K_p$  increases, the rising time decreases. But overshoot happens when  $K_p = 20$ . The rising time is also limited by the maximum voltage 12 V (thus limited maximum power). Figure 7(c) shows that the applied power spikes and decays to achieve a step response for the TCA's displacement. Note that the steady-state of the power is a

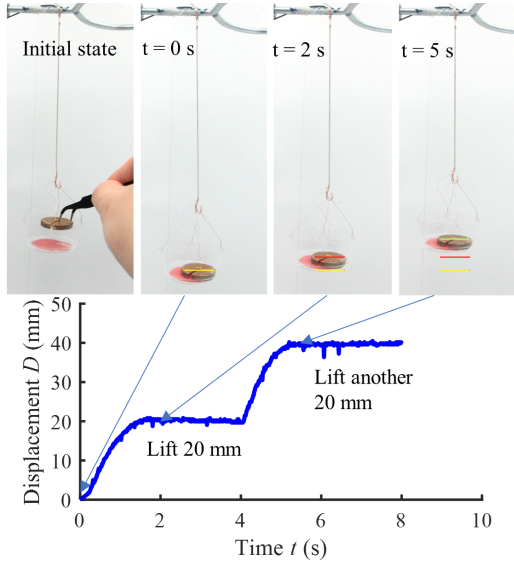


Fig. 8: The sequential snapshots and the displacement of TCA lifting a 20 g weight twice with a PI controller.

nonzero constant to maintain the position of the weight.

Since a TCA is a thermal-driven actuator, its performance subjects to the influence of the environmental temperature. The open-loop control based on modeling [16] will be greatly influenced by environmental disturbance. But a closed-loop control can actively reject the disturbance from the environment. The black line in Fig. 7(b) shows the TCA ( $K_P = 20, K_I = 0.02$ ) can reject a disturbance – blowing air that cools down the TCA faster, which decreases the TCA’s displacement. More energy is input to the TCA to maintain the displacement (black line) as shown in Fig. 7(c).

#### B. An innervated TCA with Integrated Sensing and Actuation

Combining the sensing capability while a TCA is actuated and not actuated, we further demonstrate a TCA as an innervated actuator – the TCA will first sense the weight manually added and then respond according to the weight. As shown in Fig. 8, when a 20 g is added, the TCA lifts the weight 20 mm twice (total 40 mm); when a 40 g is applied, the actuator lifts the weight 40 mm and then holds the position.

#### V. AN INNERVATED SOFT FINGER

The TCA not only can actuate a soft finger but also enable the finger to sense and respond accordingly. In the following, the design and fabrication of the finger are first introduced, and then the finger’s resistance-bending angle ( $R-\theta$ ) relationship is characterized to for the feedback control ( $\theta$  is shown in Fig. 9(c)). After that, we demonstrate that the innervated finger can sense environmental stimuli and respond to it.

#### A. Fabrication and Characterization of the Soft Finger

We fabricate our soft finger by assembling TCAs and the soft bodies (Fig. 9(a)) instead of directly embedding the

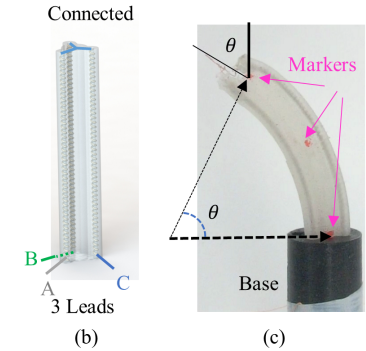


Fig. 9: (a) Schematic of the soft finger. (b) The schematic shows how leads are connected. (c). The finger with markers showing the bending angle.

TCAs in the curing process of the soft material. The method allows more flexibility in arranging TCA in the soft body, and more importantly, a damaged TCA can be easily replaced.

The fabrication procedures are [14]: 1) Fabricate soft bodies with channels. 2) Assemble TCAs in the soft bodies. Based on the length of channels in a soft body, we cut all three TCAs into the same length (45 mm) and then the TCAs are sewed into the soft body passing through the channels. 3) Connect electrical leads to the TCAs. After that, we stuck the two ends of the TCAs on the body with Sil-Poxy Silicone Adhesive (Smooth-On Inc). Finally, we fix one end of the finger on a rigid base so that the other end can move freely.

To simplify the control, the three TCAs’ top end is connected and two TCAs are actuated at the same time by applying a voltage between lead A and B (Fig. 9(b)). Since the load and the displacement of the TCA are both varying, we need to first measure the relationship between the bending angle of the finger and the TCA’s resistance ( $R-\theta$  relationship) for the closed-loop control. A constant voltage (5 V) is used to actuate the finger and the bending process is recorded. The curvature  $\kappa$  is abstracted from the three markers on the body using Tracker software (<https://physlets.org/tracker/>) and the bending angle  $\theta = L\kappa$  is calculated by assuming the arc length of the finger  $L = 40$  mm does not change as shown in Fig. 9(c). A third-order polynomial is used to fit the curve and the RMSE is  $1.6337^\circ$ .

#### B. Experiments of the Innervated Soft Finger

Figure 10(a) shows the following scenario: the robot will sense an applied bending force and start to bend  $60^\circ$  and hold the configuration for 8 s. The corresponding bending angle and the resistance are shown in Fig. 10(b). In the experiments, the resistance of the finger is continuously monitored from the beginning and then the robot will be triggered (a step response of  $60^\circ$  bending) once a resistance that is lower 0.2  $\Omega$  than the initial value (6.6  $\Omega$ ) is sensed.

The bending process is also controlled by a PI controller. From the perspective of a dynamic system, the finger can bend as fast as possible when the TCA is strong enough and sufficient power is supplied. However, from the perspective

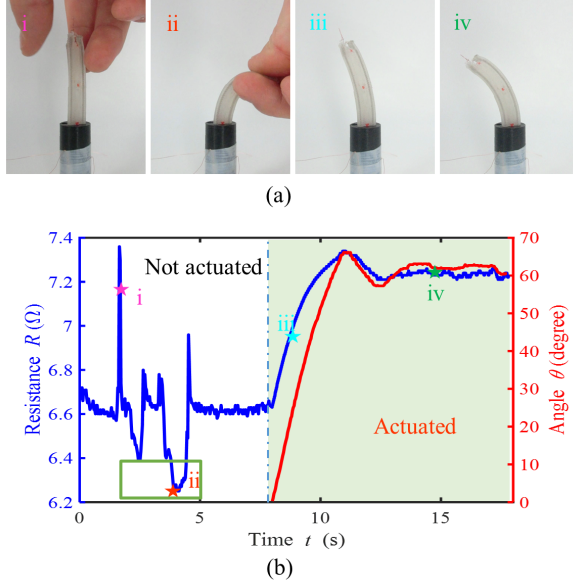


Fig. 10: (a) The snapshots of the autonomous bending finger that is triggered by external stimuli. i ,ii , iii, iv are marked with stars in (b). (b) The resistance of the soft finger and the bending angle with respect to time.

of a thermal system, it takes much longer for the finger to reach a steady-state temperature due to the relatively large heat capacity and the low thermal conductivity of the soft body. The mismatch between the motion dynamic and thermal-dynamic process of the finger causes two problems. First, it takes much longer for the finger's temperature to reach a steady state after its shape has already arrived at the target configuration. So, the TCA's surrounding temperature (soft body temperature) is changing while the finger is holding the configuration, which could be considered a disturbance. For such a reason, the finger vibrates around the target configuration, and the vibration magnitude gradually decreases as the temperature of the soft body approaches steady-state.

It is desirable that the finger can arrive at the target position as fast possible (using a large  $K_P$ ) but also guarantee the stability of the system. But this cannot be accomplished using fixed PI parameters since there is a conflict between response speed and stability. In this application, adaptive control parameters are applied to make the dynamic response faster and stable. We first use a larger  $K_P = 20$ , but tune it to be  $K_P = 3$  after the error is small enough ( $1^\circ$ ). With such a controller, the finger has a raising time around 1.5 s and steady-state error within 5% with  $K_I = 0.08$ .

## VI. CONCLUSIONS

This paper presents a framework on how to perform integrated actuation and sensing for TCAs made from conductive sewing threads. Such TCAs have an initial configuration with gaps between coils so that it can contract without preloading. Closed-loop control of the displacement is demonstrated. Leveraging the sensing function when TCA is actuated and

not actuated, we demonstrate an intelligent actuator that can perform tasks according to the external stimuli. As an application, we demonstrate a soft finger that can feel an external load and then bend to the desired angle through closed-loop control. We expect our TCAs with integrated sensing and actuation schemes can be applied to various robotic systems, especially untethered soft robots.

## REFERENCES

- [1] E. Acome, S. Mitchell, T. Morrissey, M. Emmett, C. Benjamin, M. King, M. Radakovitz, and C. Keplinger, "Hydraulically amplified self-healing electrostatic actuators with muscle-like performance," *Science*, vol. 359, no. 6371, pp. 61–65, 2018.
- [2] J. Sun, B. Tighe, and J. Zhao, "Tuning the energy landscape of soft robots for fast and strong motion," in *2020 IEEE International Conference on Robotics and Automation (ICRA)*. IEEE, 2020, pp. 10082–10088.
- [3] J. Sun, B. Pawlowski, and J. Zhao, "Embedded and controllable shape morphing with twisted-and-coiled actuators," in *2018 IEEE/RSJ International Conference on Intelligent Robots and Systems (IROS)*, 2018, pp. 5912–5917.
- [4] L. Wu, I. Chauhan, and Y. Tadesse, "A novel soft actuator for the musculoskeletal system," *Advanced Materials Technologies*, vol. 3, no. 5, p. 1700359, 2018.
- [5] A. Abbas and J. Zhao, "Twisted and coiled sensor for shape estimation of soft robots," in *2017 IEEE/RSJ International Conference on Intelligent Robots and Systems (IROS)*, Sept 2017, pp. 482–487.
- [6] X. Tang, K. Li, W. Chen, D. Zhou, S. Liu, J. Zhao, and Y. Liu, "Temperature self-sensing and closed-loop position control of twisted and coiled actuator," *Sensors and Actuators A: Physical*, vol. 285, pp. 319–328, 2019.
- [7] L. Wu and Y. Tadesse, "Modeling of the electrical resistance of tcp muscle," in *ASME 2017 International Mechanical Engineering Congress and Exposition*. American Society of Mechanical Engineers, 2017, pp. V04AT05A024–V04AT05A024.
- [8] J. van der Weijde, B. Smit, M. Fritschi, C. van de Kamp, and H. Vallery, "Self-sensing of deflection, force, and temperature for joule-heated twisted and coiled polymer muscles via electrical impedance," *IEEE/ASME Transactions on Mechatronics*, vol. 22, no. 3, pp. 1268–1275, 2016.
- [9] J. van der Weijde, H. Vallery, and R. Babuška, "Closed-loop control through self-sensing of a joule-heated twisted and coiled polymer muscle," *Soft robotics*, 2019.
- [10] S. M. Mirvakili, A. R. Ravandi, I. W. Hunter, C. S. Haines, N. Li, J. Foroughi, S. Naficy, G. M. Spinks, R. H. Baughman, and J. D. Madden, "Simple and strong: Twisted silver painted nylon artificial muscle actuated by joule heating," in *Electroactive Polymer Actuators and Devices (EAPAD) 2014*, vol. 9056. International Society for Optics and Photonics, 2014, p. 90560I.
- [11] K. Takagi, T. Arakawa, J. Takeda, K. Masuya, K. Tahara, and K. Asaka, "Position control of twisted and coiled polymer actuator using a controlled fan for cooling," in *Electroactive Polymer Actuators and Devices (EAPAD) 2017*, vol. 10163. International Society for Optics and Photonics, 2017, p. 101632V.
- [12] M. C. Yip and G. Niemeyer, "On the control and properties of supercoiled polymer artificial muscles," *IEEE Transactions on Robotics*, vol. 33, no. 3, pp. 689–699, 2017.
- [13] A. Simeonov, T. Henderson, Z. Lan, G. Sundar, A. Factor, J. Zhang, and M. Yip, "Bundled super-coiled polymer artificial muscles: Design, characterization, and modeling," *IEEE Robotics and Automation Letters*, vol. 3, no. 3, pp. 1671–1678, 2018.
- [14] J. Sun, B. Tighe, Y. Liu, and J. Zhao, "Twisted-and-coiled actuators with free strokes enable soft robots with programmable motions," *Soft Robotics*, 2020.
- [15] B. Pawlowski, J. Sun, J. Xu, Y. Liu, and J. Zhao, "Modeling of soft robots actuated by twisted-and-coiled actuators," *IEEE/ASME Transactions on Mechatronics*, 2018.
- [16] K. Masuya, S. Ono, K. Takagi, and K. Tahara, "Feedforward control of twisted and coiled polymer actuator based on a macroscopic nonlinear model focusing on energy," *IEEE Robotics and Automation Letters*, vol. 3, no. 3, pp. 1824–1831, 2018.